


Imaging Through a Fano-Resonant Dielectric Metasurface Governed by Quasi-bound States in the Continuum

Chaobiao Zhou^{1,*}, Xiaoying Qu,¹ Shuyuan Xiao,² and Menghui Fan^{1,†}

¹College of Mechanical and Electronic Engineering, Guizhou Minzu University, Guiyang 550025, China

²Institute for Advanced Study, Nanchang University, Nanchang 330031, China

 (Received 4 February 2020; revised 23 July 2020; accepted 25 August 2020; published 7 October 2020)

Fano resonance has attracted great attention in nanophotonics attributed to its unique properties. In this work, we study the imaging function of a Fano-resonant silicon metasurface governed by quasi-bound states in the continuum (quasi-BICs). First, by breaking the in-plane symmetry of nanodisks, a symmetry-protected quasi-BIC is excited with the emergence of a sharp Fano resonance. The near-field distributions, multipole contributions, and radiation patterns of the metasurface are investigated to uncover the mechanism and characteristics of this resonance. In addition, we investigate the imaging function of this Fano-resonant metasurface assisted by phase-change material $\text{Ge}_2\text{Sb}_2\text{Te}_5$ (GST). Through selective modification of different units from *a*-GST to *c*-GST, the produced transmitted image well reconstructs the target letter. Our findings may provide a route to achieve efficient metasurface-based imaging and fast spatial modulations.

DOI: [10.1103/PhysRevApplied.14.044009](https://doi.org/10.1103/PhysRevApplied.14.044009)

I. INTRODUCTION

Resonant metasurfaces have received extensive attention due to their sharp spectral feature and extraordinary field enhancement [1,2]. Early resonant metasurfaces, consisting of dielectric layers and metal films, exhibit relatively broad resonances and low transmission in the optical range due to high inherent energy dissipation of metals [3]. In recent years, all-dielectric metasurfaces with a high refractive index have become an alternative choice in nanophotonics, due to their low dissipative losses, compatibility with semiconductor fabrication, and capabilities of trapping the optical modes within dielectric nanostructures compared with their metallic counterparts [4–10].

Bound states in the continuum (BICs) are states lying inside the continuum while remaining perfectly localized without radiation [11–18], which can facilitate the excitation of resonance in dielectric metasurfaces. Based on their mechanisms, BICs are divided into symmetry-protected BICs, accidental BICs, BICs protected by integrability, etc. [11,19]. Symmetry-protected BICs can be perturbed through oblique incidence or symmetry breaking of nanostructures via building a radiation channel between eigenmodes and the free space, and thus exciting quasi-BICs [20–30]. An accidental BIC emerges from the destructive interference of several leaky waves at the off- Γ point

through tuning the parameters of a system continuously, resulting in an accidental vanishing coupling to the radiation continuum [11,12,24]. It is noted that there are also BICs in some two-particle Hubbard models, whose confinement requires no parameter tuning and has been credited to integrability [11,31–34].

Asymmetric Fano profiles with high contrast of transmission can be excited by BICs in various metasurfaces [23]. Actively tunable Fano-resonant metasurfaces can be realized through assistance of liquid crystals [35,36], two-dimensional materials [37,38], and phase-change materials [39–43], and further enable multifunctional active metadevices. $\text{Ge}_2\text{Sb}_2\text{Te}_5$ (GST), one of the phase-change materials, has received widespread attention recently attributed to its quick response, good stability, large number of switching cycles, and significant refractive index contrast in amorphous and crystalline states [44–53]. The transition between states of GST can be induced by thermal, electrical, and optical means. Nowadays, there are several mature methods to selectively modify phase states of GST on metasurfaces, such as conductive atomic force microscopy (AFM) and laser direct writing [40,54–56]. At present, investigations of GST and Fano-resonant metasurfaces mainly focus on the switching behavior realized by the manipulation of the position and strength of resonances. Combining the tunability of GST and high contrast of transmission in Fano-resonant dielectric metasurfaces, the transmitted power at a specific wavelength can be tuned dramatically. Therefore, they also hold great potential in reconfigurable imaging, which remains scarcely explored.

*cbzhou@gzmu.edu.cn

†mhfan@gzmu.edu.cn

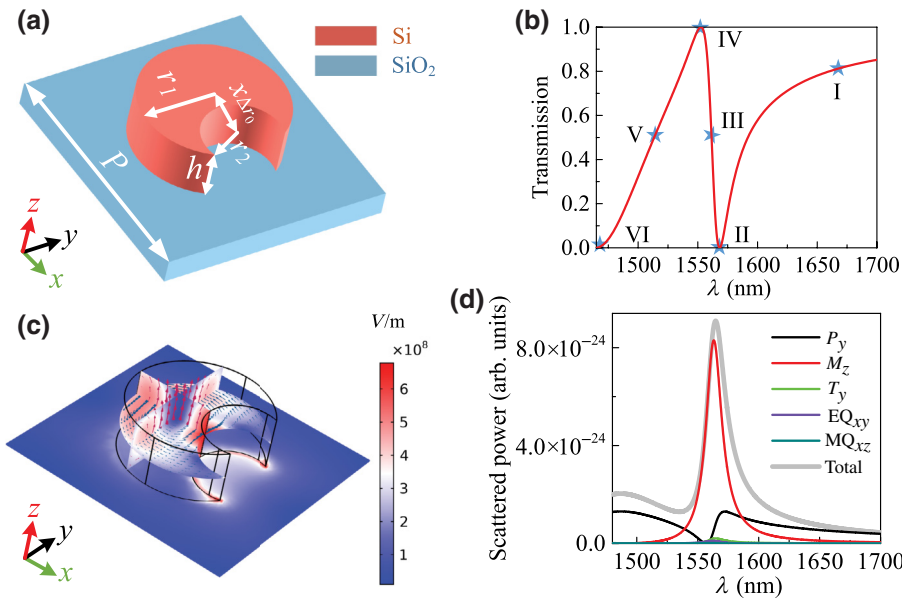


FIG. 1. (a) Geometry of a unit cell composed of an asymmetric Si nanodisk after cutting a circular notch from the edge. (b) Simulated transmission spectrum of the metasurface. (c) Electric field distributions at different cross sections in the nanodisk at the resonant wavelength. Blue arrows and red arrows represent directions of the displacement current and magnetic field, respectively. (d) The calculated scattered power of dominant multipole components.

In our work, we investigate the imaging function of a Fano-resonant dielectric metasurface supporting quasi-BICs. Firstly, we study the excitation of quasi-BICs by introducing in-plane asymmetry in highly symmetric Si nanodisks. The far-field radiation and near-field distribution are analyzed to allow an in-depth discussion. Then we discuss the tunability of the resonance through introducing a GST film to the asymmetric metasurface. Finally, after changing amorphous GST (*a*-GST) to crystalline GST (*c*-GST) at specific areas of a 40×40 array, desired patterns can be encoded in the transmitted light and reconfigurable imaging can be realized at a wavelength of 1553 nm. This active metasurface holds great potential in fast spatial modulations.

II. QUASI-BIC SUPPORTED BY ASYMMETRIC NANODISKS

A. Characteristics of the excited Fano resonance

Composite structures such as asymmetric pairs of tilted nanobars [23], split rings [57], and asymmetric nanorods [27,58] are often used to excite Fano resonances governed by quasi-BICs. However, they likely suffer from extra scattering losses from near-field coupled structures and the deep subwavelength gaps in unit cells are also difficult to fabricate accurately. Other nanostructures like notched cubes [59,60] have six sharp corners, the challenges of which in fabrication degrade the performance of resonators. Therefore, nanostructures with one resonator and fewer sharp corners per unit cell may improve the fabrication tolerance and help excite Fano resonances with better performance.

A perturbation that breaks the in-plane inversion symmetry of a structure can transform a symmetry-protected

BIC into a quasi-BIC. As shown in Fig. 1(a), cutting a circular notch at the edge of a nanodisk introduces symmetry breaking. The center distance between the nanodisk and the air-hole is $x_{\Delta r_0} = 200$ nm and the radius of the air-hole is $r_2 = 160$ nm. The nanodisk with a height of $h = 220$ nm and a radius of $r_1 = 290$ nm lies on a SiO₂ substrate with a constant lattice of $P = 1 \mu\text{m}$. A finite-element method (COMSOL Multiphysics) and finite-difference time-domain method (FDTD Solutions) are implemented to analyze the optical properties of metasurfaces. A *y*-polarized light is normally incident on metasurfaces along the *z* direction. The periodical boundary conditions are set in the *x* and *y* directions and perfectly matched layers are set in the *z* direction. The dielectric constants of Si and SiO₂ are extracted from Palik Handbook [61]. The calculated transmission spectrum is illustrated in Fig. 1(b), manifesting a sharp asymmetric Fano resonance with a maximum transmission of 1 and a minimum of 0. The actual resonant wavelength of 1561 nm is located exactly at half the distance between the maximum and minimum. Here we analyze the formation of Fano resonance in detail. After cutting a notch at the edge of the nanodisk, the electric dipole along the *y* direction (P_y) produced by the incident polarization will exhibit slightly different dipole strengths in the notch part and the opposite side. These two asymmetric dipoles will generate a *z*-directed magnetic field near the center of the nanodisk, giving rise to a *z*-polarized magnetic dipole (M_z). Finally, the broken symmetry induces interference between the in-plane electric dipole P_y and the magnetic dipole M_z , leading to the observed Fano resonance.

The simulated electric field distributions at the resonant wavelength of 1561 nm are shown in Fig. 1(c), with monitors placed at $z = 110$ nm, $y = 0$, and $x = -100$ nm to detect fields in the nanostructure. The polarization of the

electric field is anti-parallel at opposite sides of the breaking nanodisk induced by the varied effective refractive index of the silicon metasurface. This results in a distinct circular displacement current inside the nanodisk as represented by the blue arrows in the x - y plane, revealing that the energy within the metasurface is strongly trapped by the magnetic dipole moment oscillation along the z axis illustrated by red arrows in the center of the nanodisk. In order to study the excitation of this Fano resonance, electromagnetic multipole expansion under the Cartesian coordinate is performed, with the calculated scattered power shown in Fig. 1(d). At the resonance region, the M_z component makes a pronounced contribution, while other multipoles are dramatically suppressed. For the off-resonance region, the P_y component dominates. These results validate the above discussion of Fano excitation.

B. Far-field radiation patterns

We select six typical wavelengths near the Fano resonance as denoted by blue stars and Roman numerals in Fig. 1(b) to compare far-field radiation patterns. Figure 2 illustrates the far-field radiation patterns at wavelengths $\lambda_I = 1671$ nm, $\lambda_{II} = 1568$ nm, $\lambda_{III} = 1561$ nm, $\lambda_{IV} = 1553$ nm, $\lambda_V = 1514$ nm, and $\lambda_{VI} = 1465$ nm. These patterns are drawn using COMSOL Multiphysics. For the resonant wavelength $\lambda_{III} = 1561$ nm shown in Fig. 2(c), where magnetic dipole along the z axis plays a predominant role, the far-field radiation pattern mainly expands in the x - y plane. A noticeable contribution from electric dipole moment along the y axis breaks the symmetry of scattering along the x and y directions, resulting in a stronger side-scattering directed along the polarization direction of the electric field, and also produces a weak power leakage along the z axis. It is noteworthy that the far-field radiation power reaches a maximum at this actual resonant wavelength, as verified in the multipole expansion of Fig. 1(d). For neighboring wavelengths $\lambda_{II} = 1568$ nm and $\lambda_{IV} = 1553$ nm shown in Figs. 2(b) and 2(d), the contribution from originally dominant M_z decreases, and its scattered power becomes comparable with that of P_y . Therefore, P_y manifests itself in the far-field radiation by perturbing the symmetry of the radiation pattern at the resonance point and producing more leakage in the z direction. The radiation power is reduced as well. As the wavelength further increases from the resonant position, reaching $\lambda_I = 1671$ nm as illustrated in Fig. 2(a), the interaction of several multipoles (especially electric dipole and magnetic dipole) leads to a very large difference between forward scattering and backward scattering. Contributions from these nonresonant multipoles give rise to a further suppression of total scattering as well. When reducing the wavelength to the off-resonance region, corresponding to $\lambda_V = 1514$ nm shown in Fig. 2(e), the scattered power from M_z dramatically decreases, and then P_y becomes the

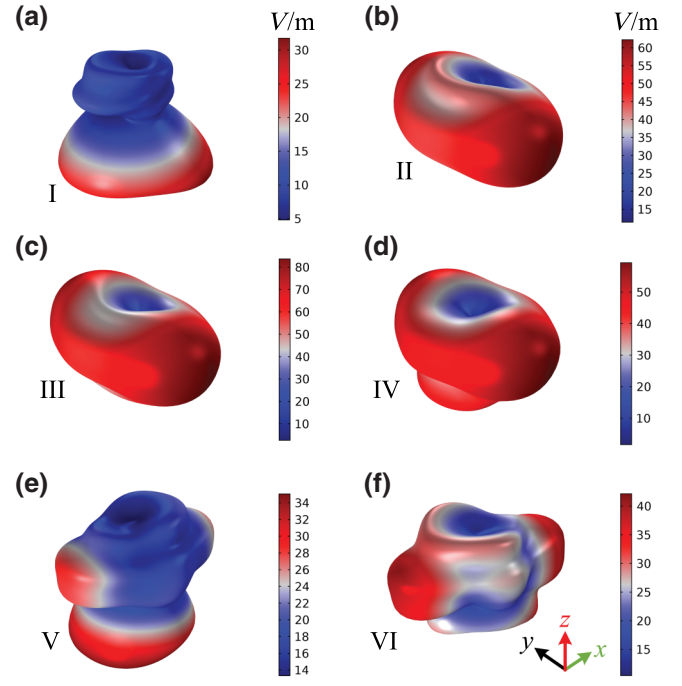


FIG. 2. Radiation patterns of metasurface composed of asymmetric nanodisks at different wavelengths: (a) $\lambda_I = 1671$ nm; (b) $\lambda_{II} = 1568$ nm; (c) $\lambda_{III} = 1561$ nm; (d) $\lambda_{IV} = 1553$ nm; (e) $\lambda_V = 1514$ nm; (f) $\lambda_{VI} = 1465$ nm.

most contributive component. Two radiation lobes along the x axis emerge and the forward scattering exhibits an enhancement. When further deviating from the resonance as depicted in Fig. 2(f) at $\lambda_{VI} = 1465$ nm, the contribution from magnetic dipole becomes negligible, and thus the enhancement of forward scattering nearly disappears. In a word, the analysis of far-field radiation patterns can not only reveal the physical mechanism between BIC and quasi-BIC, but also help to manipulate the radiation direction of the metasurface, which will finally benefit the performance of imaging.

III. IMAGING THROUGH A GST-ASSISTED FANO-RESONANT METASURFACE

In order to realize reconfigurable imaging using the Fano-resonant metasurface, we introduce a GST film on the nanodisk to manipulate the transmitted power at a specific wavelength, which is caused by the shift of resonance when GST transitions from a -GST to c -GST. The tunable characteristics of Fano resonance and the performance of Fano-resonance-based imaging are demonstrated and discussed below.

A. Active Fano resonance in the Si/GST metasurface

Herein, we add a GST film with a thickness of 20 nm on the metasurface discussed above with all other parameters remaining the same, as shown in Fig. 3(a). The optical

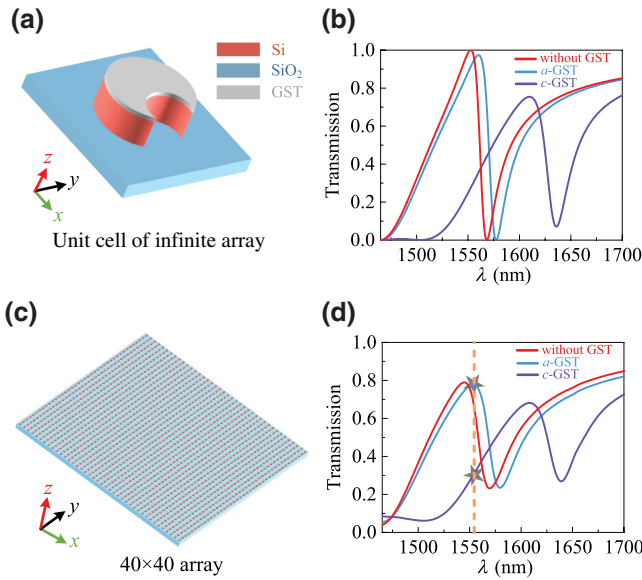


FIG. 3. (a) Geometry of a unit cell of an infinite array with Si/GST asymmetric nanodisks. (b) Simulated transmission spectra of the infinite array. (c) Geometry of a 40×40 array with Si/GST asymmetric nanodisks. (d) Simulated transmission spectra of the 40×40 array.

properties of GST are extracted from Ref. [47]. At the same simulation configurations, the calculated transmissions are illustrated in Fig. 3(b). When adding an a -GST layer on the metasurface, the Fano resonance exhibits a slight red-shift compared to the transmission without GST, which is due to the increased effective refractive index of the structure introduced by the GST film. The slightly reduced extinction ratio and broadened resonance are ascribed to the additional absorption introduced by a -GST [46]. After changing a -GST to c -GST, the resonance wavelength increases by about 50 nm due to the much larger refractive index of c -GST. In addition, the extinction ratio of the resonance suffers from an obvious reduction, provided by the growing absorption of c -GST given its larger extinction coefficient.

To make the numerical calculation more tractable, we focus our investigation of imaging on a metasurface composed of 40×40 nanodisks. By setting the boundary conditions in the x and y directions as perfectly matched layers, we calculate the transmissions of this 40×40 array [Fig. 3(c)] at a -GST and c -GST states shown in Fig. 3(d). An obvious reduction of extinction ratio is observed compared with Fig. 3(b), which can be ascribed to the array effect [59,62,63]. The resonance shown in Fig. 3(b) is excited by a unit cell with periodic boundaries in both x and y directions, which corresponds to an infinite array. As magnetic dipoles along the z axis supported by each unit coherently oscillate perpendicular to the array plane, they cancel each other and the resonance only scatters at edges of the metasurface. When the array becomes smaller than

the 40×40 array, the scattering losses grow and the resonance becomes weaker due to scattering losses of magnetic dipole radiation. It is noted that the resonance at the a -GST state is influenced more strongly by the array effect compared with that at the c -GST state, the reason for which lies in the sharper resonance of the a -GST state.

B. Reconfigurable imaging

We choose an array consisting of 40×40 nanodisk units as shown in Fig. 3(c) to balance the imaging performance and simulation capacity. The operation wavelength is set at 1553 nm [denoted by the yellow dashed line in Fig. 3(d)], the transmission maximum at the a -GST state. Thus when GST transitions from the amorphous state to the crystalline state, the corresponding transmission changes from 0.78 to 0.29 (marked by stars). We use letters “GZMU” as target images to demonstrate the imaging function of our active metasurface. First, each image of letters is discretized and then represented by a binary matrix with a size of 40×40 , with pixels corresponding to the letter part valued 1 and other pixels valued 0. Then phase states of GST on units of the metasurface are altered based on the target image matrix. This selective modification of GST phase states can be achieved in experiment through laser direct writing, conductive AFM, and so on [54–56]. For matrix pixels with values of 0, the corresponding a -GST is changed to c -GST, and thus the transmitted power from them becomes weaker compared with the other areas covered by a -GST, which manifests the desired pattern on the transmitted region. We place a field distribution monitor $10 \mu\text{m}$ away from the metasurface in the transmitted region to capture and record the power distribution of images, which is defined as the square of electric field abstract value. All these target and transmitted images are shown in Fig. 4, with each image normalized to itself. When the incident polarization relative to the target images shown in this figure is along the perpendicular direction, the transmitted images are as shown in Figs. 4(e)–4(h). All targets are clearly imaged, with power at corresponding positions of letter pixels significantly enhanced with respect to the background part. At edges of imaged letters, the power is relatively weak with no obvious boundaries with the background like that in targets. That is because the destructive interference between a -GST pixels and c -GST pixels cuts down the power at their interface. There are also alternating bright and dark stripes in the imaging region, which can be ascribed to the constructive and destructive interference of light scattered from different units. Imaging performances are also influenced by shapes of target letters. At crossing points of features in letters, where more a -GST units are included, the collected power is stronger. This results from the enhanced constructive interference in these larger areas of a -GST units with the same

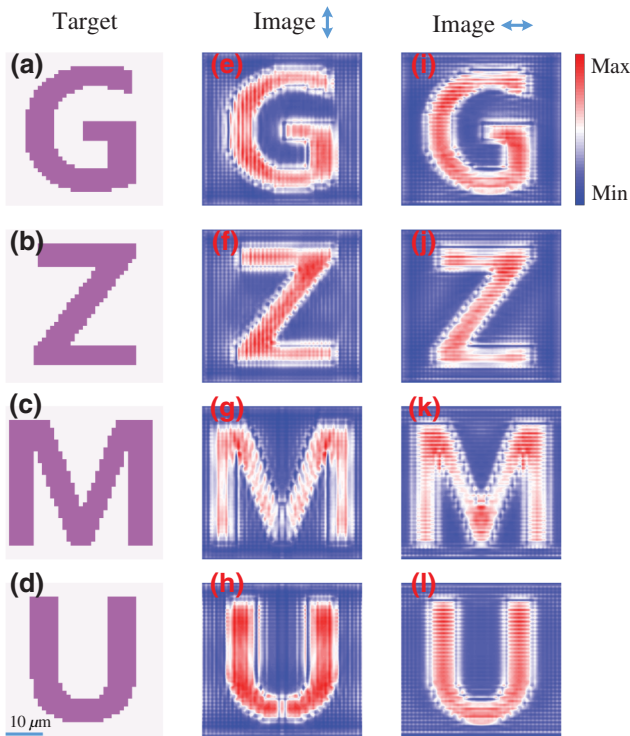


FIG. 4. (a)–(d) Target images of letters used to perform the imaging function using metasurfaces. (e)–(h) Produced transmitted images when the incident light is polarized along the perpendicular direction with respect to targets. (i)–(l) Produced transmitted images when the incident light is polarized along the horizontal direction with respect to targets. Sizes of images are all $40 \times 40 \mu\text{m}^2$, with the scale bar marked by the blue line.

amplitude and phase responses. Features along the polarization direction are more distinguishable with more power accumulated, which indicates an anisotropic response of imaging. For the letter “M”, its pixel distribution may play an important role for relatively weak imaging. Because there exists diffraction at the boundary of the metasurface, the profile of transmitted light will be redistributed due to the interference between this diffraction effect and the light steering effects supported by unit cells, tailoring the relative intensities in the detected position. Given that the left and right sides in “M” approach the edge of the metasurface, it may be more sensitive to the diffraction effect and thus be perturbed more obviously by the redistribution phenomenon.

It is noted that our designed metasurface is polarization dependent, where the Fano resonance can only be excited by incident polarization perpendicular to the symmetry axis of the nanodisk in the x - y plane. So this imaging function can only be performed under incident light polarized along the y axis. Through rotating target images while keeping the incident polarization unchanged, we also investigate the response of the metasurface when

the incident polarization is along the horizontal direction with respect to targets, with the results depicted in Figs. 4(i)–4(l). Transmitted image patterns can still be observed clearly. For the target letter “U”, the produced image is not as strong and distinct as that for another polarization, the reason for which may lie in the weakened power along the perpendicular direction when the incident light is polarized along the horizontal direction.

The imaging function of this metasurface is tunable and reconfigurable given that GST can transition from amorphous to crystalline state for a large number of cycles in just a few nanoseconds. So through selectively modifying the phase states of GST between a -GST and c -GST to form different patterns, this metasurface can realize reconfigurable imaging with high speed.

IV. CONCLUSIONS

In summary, we investigate the imaging function of a dielectric metasurface supporting a strong Fano resonance. First, we demonstrate that this Fano resonance is governed by the excitation of quasi-BICs, through breaking the in-plane symmetry of nanodisks to perturb the symmetry-protected BICs. Then near-field distributions and far-field multipole contributions are used to validate the dominant role of magnetic dipole along the z axis in the excitation of Fano resonance. Radiation patterns in the far field are depicted for several wavelengths near the resonance to further analyze resonant characteristics. Next, after adding a GST film on the metasurface, we discuss its imaging function in detail. We begin by analyzing the transmission properties of this Si/GST metasurface. Then we use a 40×40 array to produce transmitted images of targets via selectively modifying phase states of GST at different units from a -GST to c -GST, which well reconstruct corresponding targets. Our work may open up a route for metasurface-based imaging and spatial light modulation with good performance.

ACKNOWLEDGMENTS

The authors thank Dr. Shiyu Li and Professor Jiangtao Liu for fruitful discussions. This work is supported by the National Natural Science Foundation of China (NSFC) (12004084, 11764008, 11947065); Natural Science Research Project of Guizhou Minzu University (GZMU[2019]YB22, GZMU[2019]YB30); and Science and Technology Foundation of Guizhou Province and Guizhou Minzu University (LKM[2012]25).

- [1] A. E. Miroshnichenko, S. Flach, and Y. S. Kivshar, Fano resonances in nanoscale structures, *Rev. Mod. Phys.* **82**, 2257 (2010).

- [2] M. F. Limonov, M. V. Rybin, A. N. Poddubny, and Y. S. Kivshar, Fano resonances in photonics, *Nat. Photonics* **11**, 543 (2017).
- [3] J. B. Khurgin, How to deal with the loss in plasmonics and metamaterials, *Nat. Nanotechnol.* **10**, 2 (2015).
- [4] A. I. Kuznetsov, A. E. Miroshnichenko, M. L. Brongersma, Y. S. Kivshar, and B. Luk'yanchuk, Optically resonant dielectric nanostructures, *Science* **354**, aag2472 (2016).
- [5] S. Jahani and Z. Jacob, All-dielectric metamaterials, *Nat. Nanotechnol.* **11**, 23 (2016).
- [6] L. Huang, Y. Yu, and L. Cao, General modal properties of optical resonances in subwavelength nonspherical dielectric structures, *Nano Lett.* **13**, 3559 (2013).
- [7] W. Liu, A. E. Miroshnichenko, and Y. S. Kivshar, Q -factor enhancement in all-dielectric anisotropic nanoresonators, *Phys. Rev. B* **94**, 195436 (2016).
- [8] A. Sayanskiy, A. S. Kupriianov, S. Xu, P. Kapitanova, V. Dmitriev, V. V. Khardikov, and V. R. Tuz, Controlling high- Q trapped modes in polarization-insensitive all-dielectric metasurfaces, *Phys. Rev. B* **99**, 085306 (2019).
- [9] V. R. Tuz, V. V. Khardikov, A. S. Kupriianov, K. L. Domina, S. Xu, H. Wang, and H.-B. Sun, High-quality trapped modes in all-dielectric metamaterials, *Opt. Express* **26**, 2905 (2018).
- [10] V. R. Tuz, P. Yu, V. Dmitriev, and Y. S. Kivshar, Magnetic Dipole Ordering in Resonant Dielectric Metasurfaces, *Phys. Rev. Appl.* **13**, 044003 (2020).
- [11] C. W. Hsu, B. Zhen, A. D. Stone, J. D. Joannopoulos, and M. Soljačić, Bound states in the continuum, *Nat. Rev. Mater.* **1**, 16048 (2016).
- [12] C. W. Hsu, B. Zhen, J. Lee, S.-L. Chua, S. G. Johnson, J. D. Joannopoulos, and M. Soljačić, Observation of trapped light within the radiation continuum, *Nature* **499**, 188 (2013).
- [13] A. A. Bogdanov, K. L. Koshelev, P. V. Kapitanova, M. V. Rybin, S. A. Gladyshev, Z. F. Sadrieva, K. B. Samusev, Y. S. Kivshar, and M. F. Limonov, Bound states in the continuum and Fano resonances in the strong mode coupling regime, *Adv. Photonics* **1**, 016001 (2019).
- [14] A. Kodigala, T. Lepetit, Q. Gu, B. Bahari, Y. Fainman, and B. Kanté, Lasing action from photonic bound states in continuum, *Nature* **541**, 196 (2017).
- [15] S. T. Ha, Y. H. Fu, N. K. Emani, Z. Pan, R. M. Bakker, R. Paniagua-Domínguez, and A. I. Kuznetsov, Directional lasing in resonant semiconductor nanoantenna arrays, *Nat. Nanotechnol.* **13**, 1042 (2018).
- [16] L. Carletti, K. Koshelev, C. De Angelis, and Y. Kivshar, Giant Nonlinear Response at the Nanoscale Driven by Bound States in the Continuum, *Phys. Rev. Lett.* **121**, 033903 (2018).
- [17] J. Jin, X. Yin, L. Ni, M. Soljačić, B. Zhen, and C. Peng, Topologically enabled ultrahigh- Q guided resonances robust to out-of-plane scattering, *Nature* **574**, 501 (2019).
- [18] S. I. Azzam, V. M. Shalaev, A. Boltasseva, and A. V. Kildishev, Formation of Bound States in the Continuum in Hybrid Plasmonic-Photonic Systems, *Phys. Rev. Lett.* **121**, 253901 (2018).
- [19] K. Koshelev, G. Favraud, A. Bogdanov, Y. Kivshar, and A. Fratallocchi, Nonradiating photonics with resonant dielectric nanostructures, *Nanophotonics* **8**, 725 (2019).
- [20] L. Cong and R. Singh, Symmetry-protected dual bound states in the continuum in metamaterials, *Adv. Opt. Mater.* **7**, 1900383 (2019).
- [21] J. Lee, B. Zhen, S.-L. Chua, W. Qiu, J. D. Joannopoulos, M. Soljačić, and O. Shapira, Observation and Differentiation of Unique High- Q Optical Resonances Near Zero Wave Vector in Macroscopic Photonic Crystal Slabs, *Phys. Rev. Lett.* **109**, 067401 (2012).
- [22] Z. Sadrieva, K. Frizyuk, M. Petrov, Y. Kivshar, and A. Bogdanov, Multipolar origin of bound states in the continuum, *Phys. Rev. B* **100**, 115303 (2019).
- [23] K. Koshelev, S. Lepeshov, M. Liu, A. Bogdanov, and Y. Kivshar, Asymmetric Metasurfaces with High- Q Resonances Governed by Bound States in the Continuum, *Phys. Rev. Lett.* **121**, 193903 (2018).
- [24] S. Li, C. Zhou, T. Liu, and S. Xiao, Symmetry-protected bound states in the continuum supported by all-dielectric metasurfaces, *Phys. Rev. A* **100**, 063803 (2019).
- [25] Z. Liu, Y. Xu, Y. Lin, J. Xiang, T. Feng, Q. Cao, J. Li, S. Lan, and J. Liu, High- Q Quasibound States in the Continuum for Nonlinear Metasurfaces, *Phys. Rev. Lett.* **123**, 253901 (2019).
- [26] A. S. Kupriianov, Y. Xu, A. Sayanskiy, V. Dmitriev, Y. S. Kivshar, and V. R. Tuz, Metasurface Engineering Through Bound States in the Continuum, *Phys. Rev. Appl.* **12**, 014024 (2019).
- [27] E. Mikheeva, K. Koshelev, D.-Y. Choi, S. Kruk, J. Lumeau, R. Abdeddaim, I. Voznyuk, S. Enoch, and Y. Kivshar, Photosensitive chalcogenide metasurfaces supporting bound states in the continuum, *Opt. Express* **27**, 33847 (2019).
- [28] K. Koshelev, Y. Tang, K. Li, D.-Y. Choi, G. Li, and Y. Kivshar, Nonlinear metasurfaces governed by bound states in the continuum, *ACS Photonics* **6**, 1639-1644 (2019).
- [29] Y. He, G. Guo, T. Feng, Y. Xu, and A. E. Miroshnichenko, Toroidal dipole bound states in the continuum, *Phys. Rev. B* **98**, 161112 (2018).
- [30] X. Wang, S. Li, and C. Zhou, Polarization-independent toroidal dipole resonances driven by symmetry-protected BIC in ultraviolet region, *Opt. Express* **28**, 11983 (2020).
- [31] J. Zhang, D. Braak, and M. Kollar, Bound States in the Continuum Realized in the One-Dimensional Two-Particle Hubbard Model with an Impurity, *Phys. Rev. Lett.* **109**, 116405 (2012).
- [32] J. Zhang, D. Braak, and M. Kollar, Bound states in the one-dimensional two-particle hubbard model with an impurity, *Phys. Rev. A* **87**, 023613 (2013).
- [33] S. Longhi and G. Della Valle, Tamm-Hubbard surface states in the continuum, *J. Phys. Condens. Mat.* **25**, 235601 (2013).
- [34] G. Della Valle and S. Longhi, Floquet-Hubbard bound states in the continuum, *Phys. Rev. B* **89**, 115118 (2014).
- [35] Z.-X. Shen, S.-H. Zhou, S.-J. Ge, W. Hu, and Y.-Q. Lu, Liquid crystal enabled dynamic cloaking of terahertz Fano resonators, *Appl. Phys. Lett.* **114**, 041106 (2019).
- [36] M. Parry, A. Komar, B. Hopkins, S. Campione, S. Liu, A. E. Miroshnichenko, J. Nogan, M. B. Sinclair, I. Brener, and D. N. Neshev, Active tuning of high- Q dielectric metasurfaces, *Appl. Phys. Lett.* **111**, 053102 (2017).

- [37] C. Zhou, G. Liu, G. Ban, S. Li, Q. Huang, J. Xia, Y. Wang, and M. Zhan, Tunable Fano resonator using multi-layer graphene in the near-infrared region, *Appl. Phys. Lett.* **112**, 101904 (2018).
- [38] G. Sun, S. Peng, X. Zhang, and Y. Zhu, Switchable electromagnetically induced transparency with toroidal mode in a graphene-loaded all-dielectric metasurface, *Nanomaterials* **10**, 1064 (2020).
- [39] T. Cao, J. Bao, L. Mao, T. Zhang, A. Novitsky, M. NietoVesperinas, and C.-W. Qiu, Controlling lateral Fano interference optical force with Au-Ge₂Sb₂Te₅ hybrid nanostructure, *ACS Photonics* **3**, 1934 (2016).
- [40] C. H. Chu, M. L. Tseng, J. Chen, P. C. Wu, Y. H. Chen, H. C. Wang, T. Y. Chen, W. T. Hsieh, H. J. Wu, G. Sun, *et al.*, Active dielectric metasurface based on phase-change medium, *Laser Photonics Rev.* **10**, 986 (2016).
- [41] Z. Zhang, J. Yang, W. Bai, Y. Han, X. He, J. Huang, D. Chen, S. Xu, and W. Xie, All-optical switch and logic gates based on hybrid Silicon-Ge₂Sb₂Te₅ metasurfaces, *Appl. Optics* **58**, 7392 (2019).
- [42] C. Zhou, S. Li, M. Fan, X. Wang, Y. Xu, W. Xu, S. Xiao, M. Hu, and J. Liu, Optical radiation manipulation of Si-Ge₂Sb₂Te₅ hybridmetasurfaces, *Opt. Express* **28**, 9690 (2020).
- [43] W. Zhu, Y. Fan, C. Li, R. Yang, S. Yan, Q. Fu, F. Zhang, C. Gu, and J. Li, Realization of a near-infrared active Fano-resonant asymmetric metasurface by precisely controlling the phase transition of Ge₂Sb₂Te₅, *Nanoscale* **12**, 8758 (2020).
- [44] Q. Wang, E. T. Rogers, B. Gholipour, C.-M. Wang, G. Yuan, J. Teng, and N. I. Zheludev, Optically reconfigurable metasurfaces and photonic devices based on phase change materials, *Nat. Photonics* **10**, 60 (2016).
- [45] S. Li, C. Zhou, G. Ban, H. Wang, H. Lu, and Y. Wang, Active all-dielectric bifocal metalens assisted by germanium antimony telluride, *J. Phys. D Appl. Phys.* **52**, 095106 (2019).
- [46] Y. Qu, Q. Li, K. Du, L. Cai, J. Lu, and M. Qiu, Dynamic thermal emission control based on ultrathin plasmonic metamaterials including phase-changing material GST, *Laser Photonics Rev.* **11**, 1700091 (2017).
- [47] A. Karvounis, B. Gholipour, K. F. MacDonald, and N. I. Zheludev, All-dielectric phase-change reconfigurable metasurface, *Appl. Phys. Lett.* **109**, 051103 (2016).
- [48] J. Zhang, Y. Zhang, Q. Hong, W. Xu, Z. Zhu, and X. Yuan, Near-infrared rewritable, non-volatile subwavelength absorber based on chalcogenide phase change materials, *Nanomaterials* **10**, 1222 (2020).
- [49] K.-K. Du, Q. Li, Y.-B. Lyu, J.-C. Ding, Y. Lu, Z.-Y. Cheng, and M. Qiu, Control over emissivity of zero-static-power thermal emitters based on phase-changing material GST, *Light Sci. Appl.* **6**, e16194 (2017).
- [50] G. Rui, C. Ding, B. Gu, Q. Gan, and Y. Cui, Symmetric Ge₂Sb₂Te₅ based metamaterial absorber induced dynamic wide-gamut structural color, *J. Optics* **22**, 085003 (2020).
- [51] Y. Qu, Q. Li, L. Cai, M. Pan, P. Ghosh, K. Du, and M. Qiu, Thermal camouflage based on the phase changing material GST, *Light Sci. Appl.* **7**, 1 (2018).
- [52] J. Tian, Q. Li, J. Lu, and M. Qiu, Reconfigurable all-dielectric antenna-based metasurface driven by multipolar resonances, *Opt. Express* **26**, 23918 (2018).
- [53] T. Cao, K. Liu, Y. Tang, J. Deng, K. Li, and G. Li, A high-index Ge₂Sb₂Te₅-based fabry-perot cavity and its application for third-harmonic generation, *Laser Photonics Rev.* **13**, 1900063 (2019).
- [54] M. L. Tseng, P. C. Wu, S. Sun, C. M. Chang, W. T. Chen, C. H. Chu, P.-L. Chen, L. Zhou, D.-W. Huang, T.-J. Yen, *et al.*, Fabrication of multilayer metamaterials by femtosecond laser-induced forward-transfer technique, *Laser Photonics Rev.* **6**, 702 (2012).
- [55] A. Leitis, A. Heßler, S. Wahl, M. Wuttig, T. Taubner, A. Tittl, and H. Altug, All-dielectric programmable huynen's metasurfaces, *Adv. Funct. Mater.* **30**, 1910259 (2020).
- [56] R. Pandian, B. J. Kooi, G. Palasantzas, J. T. De Hosson, and A. Pauza, Nanoscale electrolytic switching in phase change chalcogenide films, *Adv. Mater.* **19**, 4431 (2007).
- [57] V. Fedotov, M. Rose, S. Prosvirnin, N. Papasimakis, and N. Zheludev, Sharp Trapped-Mode Resonances in Planar Metamaterials with a Broken Structural Symmetry, *Phys. Rev. Lett.* **99**, 147401 (2007).
- [58] J. Zhang, K. F. MacDonald, and N. I. Zheludev, Near-infrared trapped mode magnetic resonance in an all-dielectric metamaterial, *Opt. Express* **21**, 26721 (2013).
- [59] S. Campione, S. Liu, L. I. Basilio, L. K. Warne, W. L. Langston, T. S. Luk, J. R. Wendt, J. L. Reno, G. A. Keeler, I. Brener, *et al.*, Broken symmetry dielectric resonators for high quality factor Fano metasurfaces, *ACS Photonics* **3**, 2362 (2016).
- [60] N. Karl, P. P. Vabishchevich, S. Liu, M. B. Sinclair, G. A. Keeler, G. M. Peake, and I. Brener, All-optical tuning of symmetry protected quasi bound states in the continuum, *Appl. Phys. Lett.* **115**, 141103 (2019).
- [61] E. D. Palik, *Handbook of Optical Constants of Solids* (Academic Press, New York, 1998), Vol. 3.
- [62] V. A. Fedotov, N. Papasimakis, E. Plum, A. Bitzer, M. Walther, P. Kuo, D. Tsai, and N. Zheludev, Spectral Collapse in Ensembles of Metamolecules, *Phys. Rev. Lett.* **104**, 223901 (2010).
- [63] Y. Yang, I. I. Kravchenko, D. P. Briggs, and J. Valentine, All-dielectric metasurface analogue of electromagnetically induced transparency, *Nat. Commun.* **5**, 5753 (2014).